

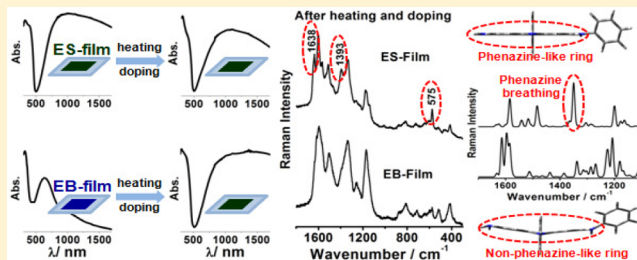
# Spectroscopic Study on the Structural Differences of Thermally Induced Cross-Linking Segments in Emeraldine Salt and Base Forms of Polyaniline

Marcelo M. Nobrega, Claudio H. B. Silva, Vera R. L. Constantino, and Marcia L. A. Temperini\*

Departamento de Química Fundamental, Instituto de Química da Universidade de São Paulo (USP), C.P. 26077- CEP 05513-970 - São Paulo, SP - Brazil

## Supporting Information

**ABSTRACT:** This paper reports the spectroscopic study on the structural differences of thermally induced cross-linking segments in polyaniline in its emeraldine salt (PANI-ES) and base (PANI-EB) forms. Casting films of PANI-ES (ES-film) and PANI-EB (EB-film) were prepared and heated at 150 °C under atmospheric air for 30 min. Raman spectra excited at 632.8 nm of heated ES-film presented the characteristic bands of phenazine-like structures at 1638, 1392, and 575 cm<sup>-1</sup>, whereas EB-film showed lower relative intensities for these bands. The lower content of phenazine-like segments in heated EB-film is related to residual polaronic segments from preparation procedures, as revealed by Raman. This statement was confirmed by a sequence of thermal and doping experiments in both films. Quantum-chemical calculations by density functional theory (DFT) and time-dependent density functional theory (TD-DFT) showed that the phenazine-like structure presents the intense Raman band at 1350 cm<sup>-1</sup> due to heterocycle breathing mode, and the non-phenazine-like structure (substituted hydrophenazine-type) presents higher energy for HOMO-LUMO transition, indicating the lack of conjugation in the heterocycle compared with the phenazine-like structure. According to experimental and theoretical data reported here, it is proposed that only thermally treated PANI-ES presents phenazine-like rings, whereas PANI-EB presents heterocyclic non-aromatic structures.



## INTRODUCTION

Among the family of conducting polymers, polyaniline (PANI) is one of the most studied due to its easy and low-cost synthesis, good environmental stability, and simple doping/dedoping process based on acid/base reactions.<sup>1–4</sup> The most known synthesis of PANI is carried out in a strong acid aqueous solution in which aniline is dissolved and the polymerization initiates by adding an oxidant, generally ammonium peroxodisulfate, into the solution at ca. 5 °C.<sup>1,2</sup> This synthetic route leads to the conducting emeraldine salt form of PANI (PANI-ES), formed by the head-to-tail coupling of the monomers. The emeraldine base form of polyaniline (PANI-EB) is obtained as a result of the dedoping of PANI-ES.<sup>5–7</sup> Scheme 1 summarizes the doping/dedoping process of PANI, which consists of a conversion of the quinoid segments of PANI-EB to polaronic segments through an internal redox reaction.<sup>5–7</sup>

Due to its good environmental stability and electrochemical properties, PANI presents interesting applications in many devices such as sensors and biosensors,<sup>8–11</sup> antistatic and anticorrosive coatings,<sup>12</sup> and batteries.<sup>13–16</sup> The study of the thermal stability of polyaniline in different doping and oxidation forms is an important subject for practical applications, because the initial step in processing procedures is performed by heating treatments.<sup>17–19</sup> The thermal properties of PANI in the doped and undoped forms have been extensively reported in

the literature.<sup>20–39</sup> Accordingly, the heating treatment causes extrinsic and intrinsic structural changes, leading to the formation of cross-linking segments in the doped and undoped forms of PANI.<sup>22–33,40</sup> The formation of these structures has been related to changes in the conductivity and crystallinity after heating.<sup>22,23,32–34,39,41</sup> The techniques used to study the thermal properties of PANI are thermogravimetric analysis (TGA) and differential scanning calorimetry (DSC), which provide macroscopic information such as decomposition temperature profile, melting point, and phase transition. However, the characterization of the type of the cross-linking formed is impossible using this technique, and spectroscopic techniques must be employed.

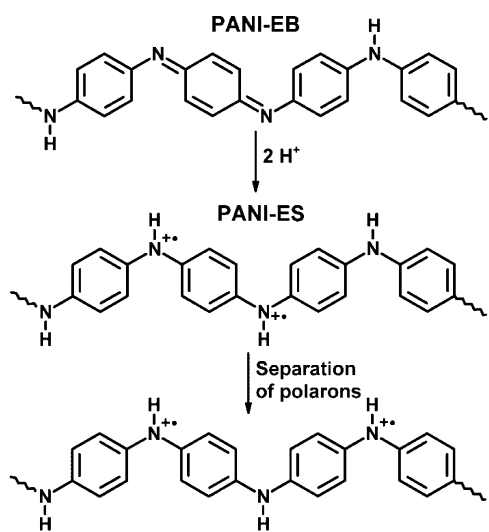
The structural characterization of thermally treated polyanilines has been generally performed by FTIR spectroscopy due to its availability,<sup>20–27,34,35</sup> but other techniques such as X-ray photoelectron spectroscopy (XPS) and nuclear magnetic resonance (<sup>13</sup>C NMR) have been used as well.<sup>21,28,35</sup> In the literature, there is a lack of consensus proposing the structures formed after heating treatment in polyaniline. Some of the different structures proposed as the cross-linking segments

Received: September 24, 2012

Revised: November 9, 2012

Published: November 11, 2012

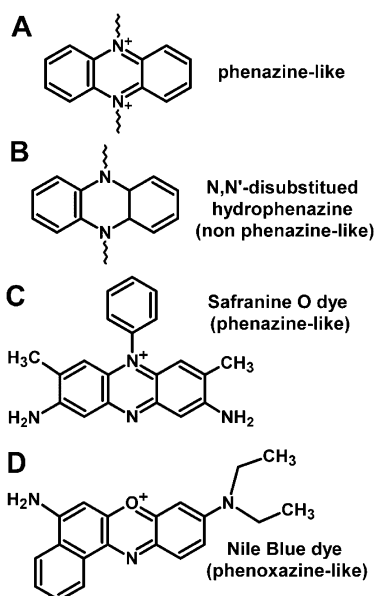
**Scheme 1. Doping Process of PANI-EB and Conversion of Quinoid Segments to Polarons in PANI-ES<sup>a</sup>**



<sup>a</sup>The anions are not shown (adapted from ref 7).

present a heterocycle ring resulting from inter- or intrachain reactions.<sup>23,27,28,30–32,39,42</sup> However, it is important to mention that many proposed structures are not proper phenazine-like rings, because they do not present the characteristic  $\pi$ -delocalization and aromaticity of the three-membered ring, as presented by the phenazine molecule.<sup>23,27,28,32,39</sup> Scheme 2 presents some of the structures proposed in the literature (A and B) as the cross-linking segments and also some heterocyclic molecules (C and D) studied for comparison as possible products of thermally treated polyaniline (adapted from refs 23, 27, 28, 30–32, 39, 42, 43). The phenazine-like and

**Scheme 2. Structures Proposed in Literature (A and B) as the Cross-Linking Segments and Heterocyclic Molecules (C and D) Also Studied for Comparison with Thermally Treated Polyaniline (adapted from refs 23, 27, 28, 30–32, 39, 42, 43)<sup>a</sup>**



<sup>a</sup>Anions not shown.

phenoxazine-like structures (A, C, and D) showed in Scheme 2 should present high conjugation, and their electronic structures are characterized by strong  $\pi-\pi^*$  transitions in the visible region (generally at longer wavelengths than 500 nm). The non-aromatic rings such as structure B (Scheme 2) should present weaker  $\pi-\pi^*$  transitions in the visible region due to the lack of conjugation in the central ring. Wu et al. reported that the ladder polymer poly(*o*-phenylenediamine) (PoPD) presents three redox states,<sup>44</sup> of which the reduced form of PoPD presents similar structure compared to the substituted dihydrophenazine in Scheme 2 (structure B). According to the authors, the reduced form of PoPD is colorless,<sup>44</sup> which clearly indicates significant differences in the electronic structure compared to the phenazine-like segments, probably due to the lack of aromaticity of the central ring.

It is well-known that resonance Raman spectroscopy is a powerful technique in the study of the different oxidation and doping forms of polyaniline. This advantage rises from the selective enhancement of the Raman bands of specific chromophoric groups by choosing the energy of the excitation radiation.<sup>45–51</sup> Wu et al. reported that only the semi and totally oxidized forms of PoPD show spectral features comparable to phenazine rings and present resonance conditions when excited at 514.5 nm radiation.<sup>44</sup> Our group has shown that resonance Raman spectroscopy is also very useful in the structural characterization of several chromophoric groups resulting from the oxidation of aniline in low acidic or alkaline media,<sup>31,52</sup> in the presence of surfactant acids,<sup>53,54</sup> or in confined environments such as inorganic hosts.<sup>55–57</sup>

This paper reports the spectroscopic study on the differences of thermally induced cross-linking segments in emeraldine salt and base forms of PANI by resonance Raman (RR) spectroscopy, supported by thermogravimetric analysis (TGA) and differential scanning calorimetry (DSC) data, as well as quantum-chemical calculations by DFT and TD-DFT. As evidenced by RR technique, only the doped samples (PANI-ES) present phenazine-like structures after heating, whereas the low content of phenazine-like in undoped samples (PANI-EB) after heating is related to residual polarons persisting after ES neutralization. From DFT and the blue shift of the band in the UV-vis-NIR spectrum of the heated EB film, the formation of a non-aromatic ring is proposed.

## EXPERIMENTAL SECTION

Aniline monomer ( $C_6H_5NH_2$ , Merck) was distilled under reduced pressure prior to use. All other chemicals (Merck) were used as received.

**Preparation of Polyaniline Powder and Dispersions of Polyaniline.** Polyaniline powder in emeraldine salt form (called "ES-powder") was prepared by the usual chemical oxidative polymerization of aniline with ammonium peroxodisulfate (APS) in 1 mol L<sup>-1</sup> hydrochloric acid at ca. 5 °C (monomer/oxidant molar ratio of ca. 4/1).<sup>1</sup> The concentrations of aniline and APS solutions were ca. 0.73 and 0.25 mol L<sup>-1</sup>, respectively. The dark green precipitate was isolated by filtration, washed with 250 mL of 1 mol L<sup>-1</sup> hydrochloric acid, and dried under reduced pressure at room temperature. Polyaniline powder in emeraldine base form (called as "EB-powder") was prepared by dedoping of 150 mg of ES-powder in 150 mL of 0.1 mol L<sup>-1</sup> NH<sub>3</sub> solution during 15 h. The solid was isolated by filtration and treated again with 150 mL of 0.1 mol L<sup>-1</sup> NH<sub>3</sub> solution for 1 h. The dark blue solid was filtered,

washed with 150 mL of 0.1 mol L<sup>-1</sup> NH<sub>3</sub> solution, and dried under reduced pressure at room temperature.

**Preparation of Glass Substrates for Casting Films of Polyaniline.** Glass substrates (2.5 cm × 2.5 cm) were cleaned according to procedures described in the literature.<sup>57,58</sup> The substrates were immersed in H<sub>2</sub>SO<sub>4</sub>/H<sub>2</sub>O<sub>2</sub> solution (7/3 in volume) for 60 min and rinsed extensively with deionized water. Afterward, the substrates were immersed in NH<sub>3</sub>/H<sub>2</sub>O<sub>2</sub>/H<sub>2</sub>O solution (5/1/1 in volume) for 30 min and rinsed extensively with deionized water. The substrates were used immediately after the cleaning.

**Preparation of Casting Films of Polyaniline in Emeraldine Base and Salt Forms.** The dispersions of polyaniline in water/N,N-dimethylacetamide (DMA) were prepared following the procedure from the literature.<sup>57,59</sup> Dedoped polyaniline powder (EB-powder) (100 mg) was slowly added to 5 mL of DMA under stirring. The solution was stirred for 12 h and filtered to remove the insoluble particles. The concentration of the resulting dark blue solution was ca. 40 × 10<sup>-3</sup> mol L<sup>-1</sup> (mol of the constitutional tetramer unit of PANI-EB), which was determined by UV-vis absorption spectroscopy considering the absorption coefficient at 630 nm ( $\epsilon_{630} = 2.20 \times 10^4$  L cm<sup>-1</sup> mol<sup>-1</sup>).<sup>60</sup> The dispersion of PANI-EB for preparation of the casting film was obtained by adding 2 mL of the PANI-EB/DMA solution to 18 mL of deionized water, resulting in a water/DMA dispersion of pH ca. 6. For preparation of the dispersion of PANI-ES, half of the dispersion of PANI-EB was carefully acidified to pH 2.5 by addition of hydrochloric acid (1 mol L<sup>-1</sup>), resulting in a water/DMA dispersion of dark green color. The acidification of the dispersion was carried out slowly to prevent the precipitation of polyaniline in medium of pH < 2.0. Finally, the casting films of polyaniline in emeraldine base and salt forms were prepared by deposition of ca. 1 mL of the respective water/DMA dispersion on clean glass substrates and drying under reduced pressure at room temperature. The casting films of PANI-EB and PANI-ES were called "EB-film" and "ES-film", respectively.

**Thermal Analyses, Heating Treatments, and Doping Process.** The mass-coupled thermogravimetric analyses (TGA-DSC-MS) of the powder polyanilines (EB-powder and ES-powder) were performed by heating the samples from room temperature to 1000 °C and by isothermal heating at 150 °C during 90 min. The TGA-DSC-MS curves were recorded on a Netzsch thermoanalyser model TGA/DSC 490 PC Luxx coupled to an Aëlos 403 C mass spectrometer, under synthetic air flow of 50 mL min<sup>-1</sup> and heating rate of 10 °C min<sup>-1</sup>. The heating treatments of the casting films EB-film and ES-film were performed in an oven under atmospheric air at 150 °C during 30 min. The temperature of 150 °C and the specific times for the thermal treatments (30 min) were chosen, based on previous tests, in order to avoid the over-dedoping of emeraldine salt samples, which could mask the Raman spectra at 632.8 nm excitation radiation, as will be discussed later. The doping of the heated casting films was carried out by exposing the samples to hydrogen chloride (HCl(g)) flow for ca. 2 min, which was generated from reaction of H<sub>2</sub>SO<sub>4</sub> (98% m/m) and KCl (s).

**Spectroscopic Characterization.** UV-vis-NIR electronic absorption spectra of the polyaniline casting films were recorded using a Shimadzu UVPC-3101 scanning spectrometer by subtracting the spectrum of glass substrate. Raman spectra at 632.8 nm excitation radiation (He-Ne laser, Renishaw 7N17S3) were obtained in a Renishaw Raman imaging

microscope (inVia) with a Leica microscope and a CCD detector, by using a 50× lens (Olympus SM Plan, N.A. 0.55). To avoid photodegradation of polyaniline samples, careful procedures were taken to record the Raman spectra at 632.8 nm. For emeraldine salt form, the samples were focused and the laser power was kept below 50 μW (power density of ca. 20 μW μm<sup>-2</sup>), and spectra were acquired using extended mode (200–1800 cm<sup>-1</sup>, 30 s, 12 accumulations). Emeraldine base samples were defocused by 10.0 μm from the working distance, so the laser power could be kept at 500 μW (power density of ca. 25 μW μm<sup>-2</sup>) for faster spectral acquisition (200–1800 cm<sup>-1</sup>, 10 s, 6 accumulations). The irradiated areas were determined by procedures reported in the literature (see Supporting Information).<sup>61</sup> Raman spectra at 1064 nm excitation radiation (Nd:YAG laser, Coherent Compass 1064–500N) were recorded in a FT-Raman Bruker RFS 100 spectrometer with a liquid-nitrogen-cooled germanium detector. The spectra were obtained using laser power of 20 mW and accumulation of 1024 scans.

**Calculation Details.** Quantum-chemical calculations were performed by using the Gaussian03 suite of programs.<sup>62</sup> The ground-state geometries of the cross-linking model structures were optimized by DFT with B3LYP hybrid functional,<sup>63–65</sup> 6-31+G(d) one-electron atomic basis sets, and no imposition of symmetry. Simulated vibrational spectra were obtained at the same level of theory employed for optimization, and no imaginary wavenumbers were obtained, which indicates that optimized geometries are in the minimum of the potential energy surfaces. Raman spectra were plotted considering a fwhm of 5 cm<sup>-1</sup>, and a scaling factor of 0.9636 for harmonic vibrational wavenumbers was used in accordance with a recent paper on the optimized scaling factors at the current functional and basis sets.<sup>66</sup> The Raman intensities were calculated from Raman activities according to the literature.<sup>67</sup> The vertical transition energies were calculated by TD-DFT protocol for the optimized geometries at the B3LYP/6-31+G(d) theory level, with the aid of the Gaussian03 package.<sup>62</sup>

## RESULTS AND DISCUSSION

The thermogravimetric analysis and differential scanning calorimetry (TGA-DSC) curves of ES-powder and EB-powder are showed in Figure 1. The ES-powder presents mainly three events of mass change (in the ranges 25–120, 120–300, and 300–700 °C), whereas EB-powder presents only two events (at 25–120 and 300–700 °C). The event in the lower temperature range for both powders is due to moiety loss,<sup>20–27,29</sup> whereas the evolution of adsorbed and unbound hydrogen chloride is also reported for ES-powder in this range of temperature.<sup>20–22,34</sup> The second and less prominent mass loss of ES-powder (150–300 °C) is attributed to loss of HCl dopant strongly bound to polyaniline chains.<sup>20–23,34,35</sup> The mass losses at high temperatures (300–700 °C) of ES-powder and EB-powder are attributed to complex and irreversible processes of decomposition of the polymeric chains.<sup>20,22–25,34,36</sup> Although the losses of moisture and dopant are endothermic events (positive heat flow),<sup>23–27,29</sup> the DSC curves in Figure 1 indicate that highly exothermic events are more important for the overall heat flow, indicating the formation of strong bonds. The results showed in Figure 1 are in agreement with reports in the literature on the thermal properties of polyanilines in air.<sup>21,25,26,34,35</sup>

The formation of cross-linking segments occurs by intra- or interchain reactions and was reported to take place at

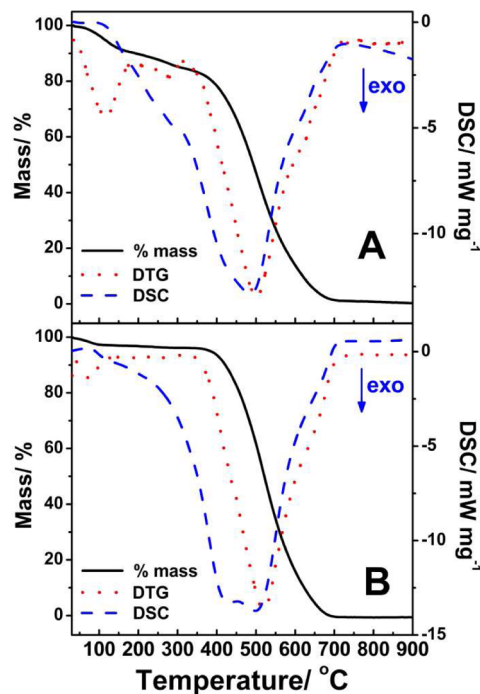


Figure 1. TGA-DSC curves of (A) ES-powder and (B) EB-powder.

intermediary temperature ranges (ca. 100–250 °C), resulting from exothermic events.<sup>23–27,29</sup> However, the overlap of several thermal events observed under the usual heating conditions (from 25 to 1000 °C) makes the evaluation of the formation of cross-linking segments difficult from the TGA-DSC curves in Figure 1. Therefore, the TGA-DSC curves obtained during the isothermal heating at 150 °C could provide additional information on specific thermal events that result in cross-linking formation.

Figure 2 shows TGA-DSC and the DTG-MS curves of ES-powder and EB-powder during the isothermal heating at 150 °C. For both polyanilines, the TGA-curves in Figure 2A,B show that most of the mass losses occur at the beginning of heating (until ca. 15 min), whereas ES-powder (Figure 2A) presents higher mass change due to dedoping process (loss of HCl) than EB-powder. The DSC curves in Figure 2A,B show the endothermic peak at the beginning of the heating process indicating the loss of moisture (and loss of dopant, for ES-powder), in accordance with the discussions above. The exothermic peaks observed at longer heating indicate the formation of cross-linking segments in both polyanilines. By comparison of the DSC curves, EB-powder presents a thinner exothermic peak with steady stabilization of heat flow at ca. -0.1 mW mg<sup>-1</sup>, whereas ES-powder shows a broader and long-tailed peak. These results could suggest different structural features of the incoming cross-linking segments in the doped and undoped forms of PANI, in addition to differences in the amount of cross-linking segments formed. Figure 2C,D show the DTG-MS curves of ES-powder and EB-powder, respectively. The DTG-MS curves at the beginning of the heating process show the detection of fragments of *m/z* ratio equal to 18 for both samples and noticeable detection of fragments of *m/z* ratio equal to 36 (at ca. 15 min) only for ES-powder. Considering that fragments of *m/z* 18 and 36 are due to H<sub>2</sub>O and HCl, respectively, Figure 2C,D indicates the loss of moisture for both polyanilines and loss of dopant only for ES-powder, in accordance with results of Figure 1. Therefore, the results of the TGA-DSC-MS technique for the isothermal heating of powder polyanilines are in accordance with results in the literature,<sup>21–23,25,35</sup> and DSC profiles suggest some different structural features of the cross-linking segments formed during the heating at 150 °C. It is also important to mention that the TGA-DSC-MS technique provides data about the most prominent thermal events, but detailed structural investigation must be performed.

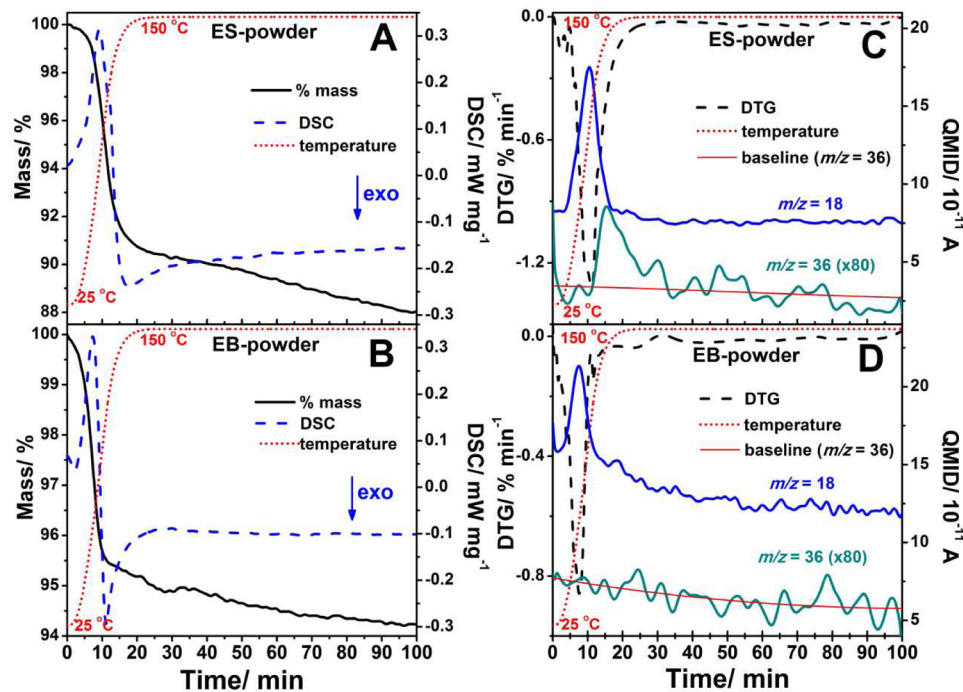
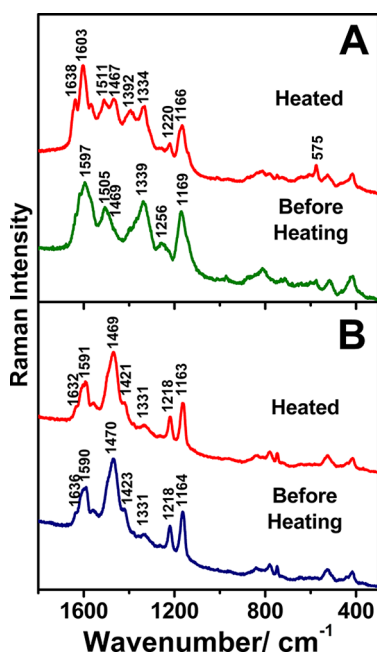


Figure 2. TGA-DSC and DTG-MS curves for the isothermal heating at 150 °C of (A and C) ES-powder and (B and D) EB-powder.

In order to characterize the cross-linking segments formed during heating, resonance Raman technique is used. For better reproducibility of the data acquisition and uniformity of the heating treatment, casting films of PANI-ES (ES-film) and PANI-EB (EB-film) forms were prepared and analyzed as described in the Experimental Section. The Raman spectra of the ES-film and EB-film before and after heating treatment are presented in Figure 3. The spectrum of ES-film presents bands



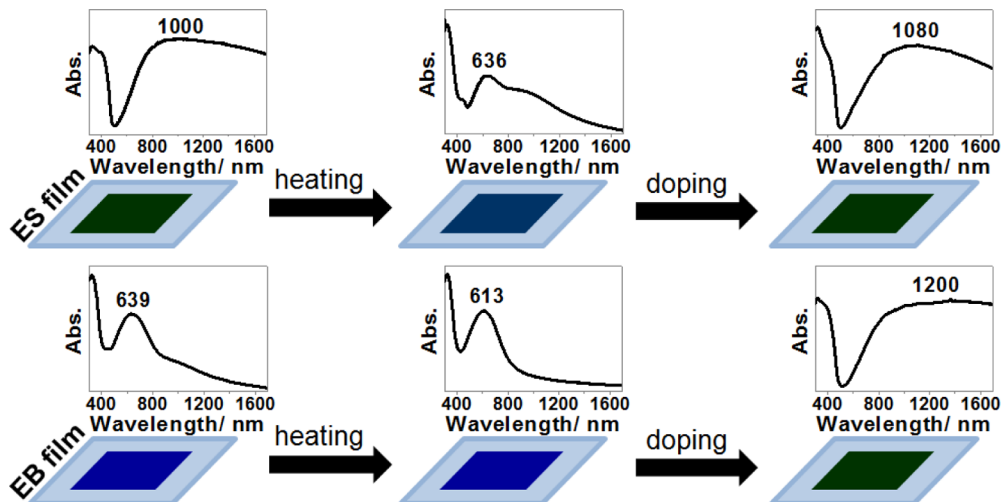
**Figure 3.** Raman spectra of the (A) ES-film and (B) EB-film before and after heating ( $\lambda_0 = 632.8 \text{ nm}$ ).

at  $1597 (\nu_{\text{C}-\text{C}})$ ,  $1505 (\nu_{\text{C}-\text{C}})$ ,  $1339 (\nu_{\text{C}-\text{N}\bullet+})$ , and  $1169 \text{ cm}^{-1} (\beta_{\text{C}-\text{H}})$  characteristic of the polaronic segments.<sup>45–49</sup> The characteristic bands of EB-film are due to the quinoid segments at  $1590 (\nu_{\text{C}-\text{C}})$ ,  $1470 (\nu_{\text{C}=\text{N}})$ ,  $1218 (\nu_{\text{C}-\text{N}})$ , and  $1164 (\beta_{\text{C}-\text{H}}) \text{ cm}^{-1}$ <sup>45–47</sup> whereas the band at ca.  $1331 \text{ cm}^{-1}$  is assigned to

residual polaronic segments in the EB-film. The Raman spectrum of the ES-film after heating treatment presents the decrease of the relative intensities of the polaron bands at  $1511$  and  $1334 \text{ cm}^{-1}$ , and the increase of the quinoid bands at  $1467$  and  $1220 \text{ cm}^{-1}$ . These results indicate the thermal dedoping of ES-film. The bands at  $1638$ ,  $1392$ , and  $575 \text{ cm}^{-1}$  in the spectrum of the heated ES-film are assigned to substituted phenazine structures.<sup>30–32,37,43,44,52,54,55,68–70</sup> These results clearly show that the thermally induced cross-linking segments in ES-film (doped polyaniline) present phenazine-like structures. The heating treatment of EB-film does not result in noticeable changes of the Raman spectrum at  $632.8 \text{ nm}$  (Figure 3B). As discussed for the TGA-DSC results (Figure 2B) and reported in the literature,<sup>22–25,28,29</sup> the heating treatment of undoped polyaniline results in some exothermic event, which may be related to formation of cross-linking segments. However, the nonobservation of any spectral changes for heated EB-film could be attributed to a different structure (and different resonance conditions) of the formed cross-linking segments compared with the phenazine-like segments observed in heated ES-film. Additionally, the strong resonance conditions of quinoid segments could make difficult the observation of Raman bands of other structures formed during the heating treatment of EB-film.

One point to be considered in this investigation is that bands of both quinoid segments of polyaniline and phenazine-like structures are enhanced at  $632.8 \text{ nm}$  excitation radiation.<sup>30–32,37,44–46,52,54,55,68–72</sup> Therefore, depending on the relative amounts of quinoid and phenazine-like segments and their enhancement factors, the structural characterization of cross-linking segments may be ambiguous or inconclusive. In order to overcome this problem and knowing that Raman bands of PANI-ES are less enhanced at  $632.8 \text{ nm}$  excitation radiation comparing to PANI-EB, one experimental procedure to verify the formation of the phenazine-like segments in PANI-EB by RR spectroscopy is to dope the samples after the heating treatments, that is, conversion of heated EB into heated ES. Therefore, in the case of thermally dedoped samples, the phenazine-like spectrum could be seen because there is no PANI-EB species after doping the heated films.

**Scheme 3. Scheme of the Experimental Procedure and UV-vis-NIR Absorption Spectra of the Casting Films before and after the Heating Treatment and Doping with HCl(g)<sup>a</sup>**



<sup>a</sup>For details of the heating treatment and doping, see Experimental Section.

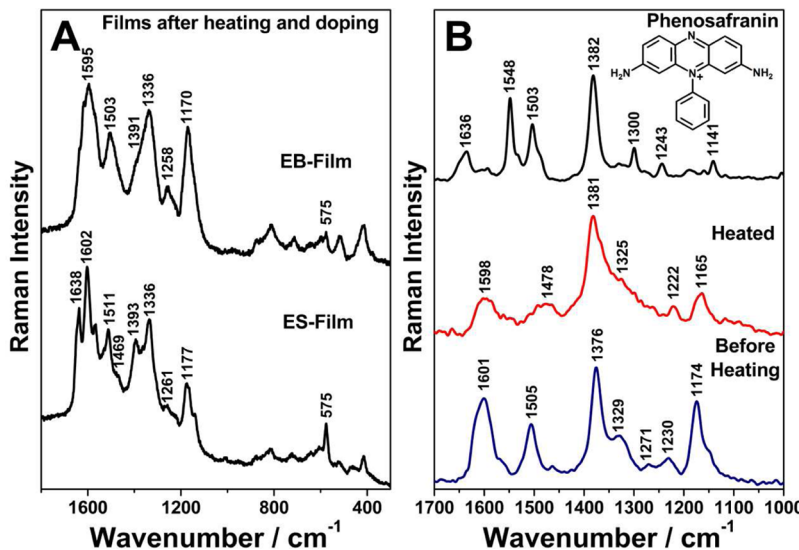


**Figure 4.** (A) Raman spectra of the films after heating and doping with  $\text{HCl(g)}$ , originating from ES-film (bottom) and EB-film (upper),  $\lambda_0 = 632.8$  nm. (B) Raman spectra of the EB-film before and after heating treatment and of Phenosafranin dye (phenazine-like structure),  $\lambda_0 = 1064$  nm.

Scheme 3 presents the experimental procedure performed to study the ES-film and EB-film and their UV-vis-NIR spectra before and after heating treatments and after doping with  $\text{HCl(g)}$ . The electronic absorption spectra of ES-film and EB-film before heating (Scheme 3) present bands at 1000 and 639 nm, respectively. The former band is attributed to the delocalized polarons,<sup>31,57,73–75</sup> whereas the latter is due to the quinoid segments of polyaniline.<sup>71,74,76,77</sup> The quinoid band of the EB-film spectrum also shows a shoulder at longer wavelengths, which suggests some residual amount of polaronic segments in EB-film. After the heating treatment, the quinoid band of EB-film shifts to 613 nm and the shoulder at longer wavelength disappears. These results indicate the disappearance of residual polarons due to thermal dedoping. For the heated ES-film, the rising of the quinoid band at 636 nm indicates thermal dedoping of the polymer, but the shoulder at longer wavelengths suggests that some residual polarons still remain in the film after heating treatment. Finally, the UV-vis-NIR spectra of both heated films after doping with  $\text{HCl(g)}$  show the intense polaron bands at the NIR region, which confirms the redoping process of polyaniline in ES-film and EB-film. According to electronic absorption spectra presented in Scheme 3, it is important to mention that using only the UV-vis-NIR technique is not able to determine the structures of the cross-linking segments.

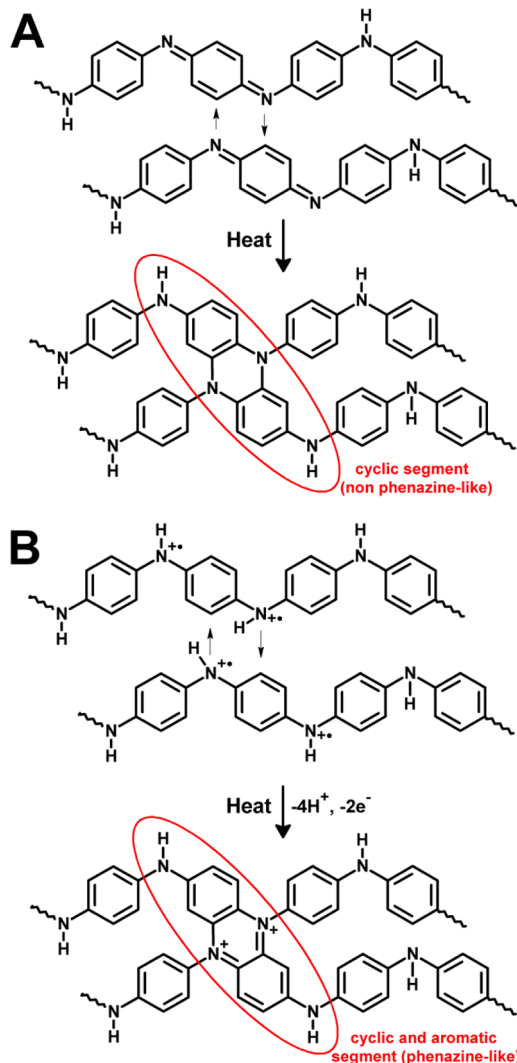
Figure 4A presents the Raman spectra of the casting films of EB and ES after heating and doping with  $\text{HCl(g)}$ . Raman spectrum of the heated ES-film after doping presents the decrease of the relative intensities of the quinoid bands at 1469 and  $1220\text{ cm}^{-1}$  and the increase of the polaron bands at 1511 and  $1336\text{ cm}^{-1}$ . These results confirm the redoping of heated ES-film, in accordance with the UV-vis-NIR spectrum (Scheme 3). The Raman bands of the phenazine-like segments at 1638, 1393, and  $575\text{ cm}^{-1}$  are also intensified after redoping the heated ES-film, which confirms that such structures are present in the thermally induced cross-linking segments. Finally, the Raman spectrum of the heated EB-film after doping presents very similar spectral features of ES-film before heating treatment (bottom spectrum of Figure 3A), which indicates the doping of polyaniline, in accordance with UV-vis-NIR spectrum (Scheme 3). It is important to notice that the

Raman spectrum of the heated EB-film after doping presents phenazine-like bands, but their relative intensities are very lower compared with ES-film (after heating and doping). This result clearly indicates that the formation of phenazine-like structures as the thermally induced cross-linking segments is not favored for the PANI-EB. In fact, the very low amount of phenazine-like structures in the heated EB-film is related only to the residual doped segments in the film, as presented in the following discussion.

Due to strong resonance conditions, the Raman bands of the polarons of polyaniline can be monitored by excitation at 1064 nm.<sup>47,48,78</sup> Therefore, even residual amounts of such segments may be identified by RR spectroscopy.<sup>79</sup> Figure 4B shows the Raman spectra of EB-film before and after heating treatment, as well as the spectrum of a phenazine-like compound, Phenosafranin dye. The Raman spectrum of the EB-film before heating treatment clearly shows the characteristic polaron bands at 1601, 1505, 1376–1329, and  $1174\text{ cm}^{-1}$ ,<sup>47,48,78,79</sup> which indicate the residual amounts of these segments in the casting film. After heating treatment, the Raman spectrum of the EB-film presents noticeable changes in the relative intensities, which suggests that the most intense band at  $1381\text{ cm}^{-1}$  could not be assigned to the polaronic segments. This result indicates that the residual amounts of polarons are consumed during the heating treatment and other structures are formed. By comparison of the Raman spectrum of the heated EB-film with Phenosafranin dye, a good accordance is observed with the band at  $1382\text{ cm}^{-1}$  of the phenazine-like molecule, assigned to the totally symmetric mode of the phenazine ring.<sup>44,80,81</sup> These results clearly show that the low amount of phenazine-like structures observed after heating treatment of the EB-film is related to the residual polarons in the casting film.

Considering the differences in the thermal behaviors between emeraldine salt and base forms of PANI, two different mechanisms could take place for the formation of cross-linking segments (Scheme 4). For the PANI-EB form, the heating treatment causes the interchain reaction from imine nitrogen atoms to quinoid rings, resulting in the cyclization processes, where the incoming rings are not aromatic. For the PANI-ES form, the cyclization process occurs by the coupling of the

**Scheme 4.** Proposed Structures of the Thermally Induced Cross-Linking Segments for the (A) Undoped and (B) Doped Forms of Polyaniline<sup>a</sup>



<sup>a</sup> Adapted from refs 23, 27, 28, 30–32, 39, 42, 43.

protonated nitrogen atoms (from polaronic segments) to benzene rings, giving phenazine-like rings as cross-linking segments, as shown in Scheme 4.

Considering some reports that PANI-EB undergoes extensive cross-linking formation after long-term thermal treatment,<sup>20,28,39</sup> EB-film was also heated for 24 h at 150 °C and doped with HCl(g). Figure 5 presents the Raman spectra of the EB-film heated during 24 h before and after the doping process, and the UV-vis-NIR spectra of the EB-film before heating and after heating for 30 min and 24 h. By comparison of the Raman spectra in Figure 5A with results in Figure 4A, it is observed that a heating treatment for a longer time does not lead to significant spectral changes. Additionally, it is observed that the Raman spectrum of the film after heating for 24 h and doping (Figure 5A) does not present intense bands due the phenazine-like segments. These results confirm that the formation of an extensive amount of phenazine-like segments does not occur at the present experimental conditions for PANI-EB even for long heating times. The UV-vis-NIR spectra in Figure 5B show that the absorption band at the visible region presents a noticeable

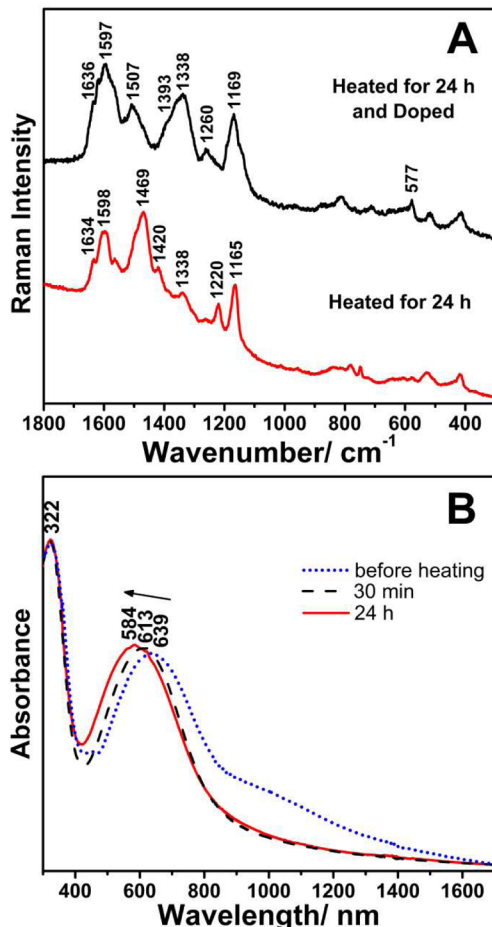


**Figure 5.** (A) Raman spectra of the EB-film heated at 150 °C for 24 h before and after doping with HCl(g) ( $\lambda_0 = 632.8 \text{ nm}$ ). (B) UV-vis-NIR spectra of the EB-film before heating and after heating for 30 min and 24 h.

shift to shorter wavelengths as a function of the time of heating at 150 °C. The blue shift of the absorption band of PANI could be attributed to oxidation from emeraldine to the pernigraniline base form (PB).<sup>50,51</sup> However, Figure 5A shows that the Raman band at  $1469 \text{ cm}^{-1}$  does not present a shift to higher wavenumber, characteristic of the formation of PB. Therefore, the blue shift observed by the UV-vis-NIR data in Figure 5B indicates the formation of cross-linking segments, which present lower conjugation in relation to phenazine-like structures, as suggested in Scheme 4.

In support of the spectroscopic characterization, quantum chemical calculations were performed by DFT to model structures based on cross-linking segments proposed in Scheme 4. Figure 6 shows the optimized geometries of the phenazine-like (aromatic) and non-phenazine-like (non-aromatic) models, as well as the calculated Raman spectra. The phenazine-like model (Figure 6A) clearly presents planarity for the three-membered ring, which is not observed in the non-phenazine-like model (Figure 6B). This result indicates that the former structure presents higher conjugation compared with the latter. The comparison of the calculated Raman spectra of the two model structures shows that the bands related to the three-membered ring present significant differences in intensity and wavenumber. These modes give rise to intense bands at 1350 (breathing mode) and  $1484 (\nu_{\text{C}-\text{C}} + \nu_{\text{C}-\text{N}}) \text{ cm}^{-1}$  for the phenazine-like model, whereas for the non-phenazine-like

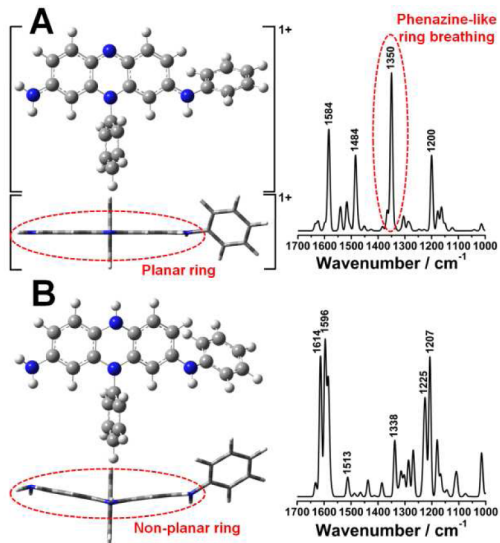


**Figure 6.** DFT optimized geometries and simulated Raman spectra of the (A) phenazine-like (aromatic) and (B) non-phenazine-like (non-aromatic) cross-linking models. B3LYP/6-31+G(d) level of theory with no imposition of symmetry. Raman spectra plotted with fwhm of 5 cm<sup>-1</sup> and scaling factor of 0.9636 for harmonic wavenumbers.

model, the bands are shifted to 1338 and 1513 cm<sup>-1</sup> and become significantly weaker. These theoretical data are in accordance with the spectroscopic data of heated films, which indicate that PANI-ES presents phenazine-like rings, whereas the PANI-EB form presents nonaromatic heterocyclic structures as thermally induced cross-linking segments.

Another observation that is in accordance with our discussions about the cross-linking segment comes from the calculated absorption energies. The vertical transition energies were calculated by TD-DFT, and Figure 7 shows the contours of the molecular orbitals involved in the lowest-energy transitions (HOMO→LUMO) of the cross-linking model structures, as well as the respective oscillator strengths ( $f$ ). TD-DFT results show that the phenazine-like structure (Figure 7A) presents lower energy for the HOMO→LUMO transition ( $\lambda = 490$  nm) compared with the non-phenazine-like structure (Figure 7B,  $\lambda = 430$  nm). These results indicate the lack of conjugation in the heterocycle of the latter structure compared with the former, in accordance with discussions presented

before. The comparison of the contours of the molecular orbitals for the lowest-energy transitions clearly shows that in the phenazine-like structure the  $\pi$ -system of the heterocycle is involved, whereas in the non-phenazine-like, the LUMO is mostly composed of the orbitals of the phenyl group. These results are in accordance with Wu et al., who showed that reduced and semi-oxidized forms of PoPD present very different electronic spectra.<sup>44</sup> Therefore, quantum chemical calculations are in accordance with the proposed differences of the electronic and vibrational structures between the cross-linking segments in the emeraldine salt and base forms of polyaniline.

## CONCLUSIONS

The thermally induced cross-linking segments in PANI-ES and PANI-EB were studied by electronic UV-vis-NIR and resonance Raman spectroscopies, and supported by thermogravimetric analysis, differential scanning calorimetry, and quantum chemical calculations. Differential scanning calorimetry indicated that both forms of PANI suffer cross-linking formation during heating at intermediate temperatures (ca. 150–250 °C). Raman spectra excited at 632.8 nm of the heated ES-film form of polyaniline presented the characteristic bands of phenazine-like structures at 1638, 1392, and 575 cm<sup>-1</sup>, whereas EB-film showed lower relative intensities for these bands. Raman spectra excited at 1064 nm revealed that the lower content of phenazine-like segments for the heated EB-film is due to residual polaronic segments. The UV-vis-NIR and Raman results of EB-films heated for 24 h at 150 °C and doped with HCl(g) indicate the formation of cross-linking segments, which present lower conjugation than phenazine-like segments. DFT calculations for non-aromatic (non-phenazine-like) and aromatic (phenazine-like) cross-linking models indicated that only the phenazine-like structure presents the Raman band at 1350 cm<sup>-1</sup> due to the heterocycle breathing mode. Moreover, TD-DFT calculations showed that the non-phenazine-like structure presents higher energy for the HOMO→LUMO transition ( $\lambda = 430$  nm) indicating the lack of conjugation in the heterocycle compared with the phenazine-like structure ( $\lambda = 490$  nm). According to experimental and theoretical data reported here, it is proposed that only thermally treated PANI-ES presents phenazine-like rings, whereas thermally treated PANI-EB presents heterocyclic

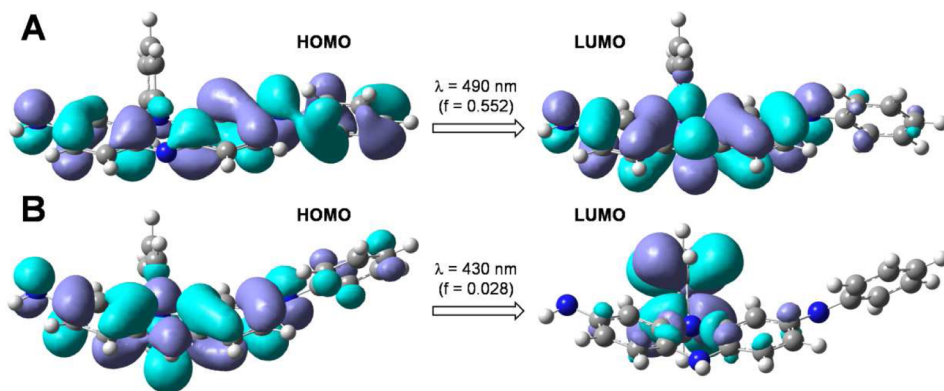


**Figure 7.** Contours of the molecular orbitals involved in the lowest-energy transitions (HOMO→LUMO) of the cross-linking model structures (A) phenazine-like and (B) non-phenazine-like, and the respective oscillator strengths ( $f$ ). Calculations from TD-DFT protocol with B3LYP/6-31+G(d) level of theory.

non-aromatic structures as the thermally induced cross-linking segments.

## ■ ASSOCIATED CONTENT

### § Supporting Information

Detailed determination of the irradiated areas during the Raman measurements according to the procedure described by Etchegoin et al.<sup>61</sup> This material is available free of charge via the Internet at <http://pubs.acs.org>.

## ■ AUTHOR INFORMATION

### Corresponding Author

\*Tel.: + 55 11 3091 3890; fax: + 55 11 3091 3890. E-mail address: mlatempe@iq.usp.br.

### Notes

The authors declare no competing financial interest.

## ■ ACKNOWLEDGMENTS

The authors acknowledge the Brazilian agencies CNPq and FAPESP for fellowships and financial support.

## ■ REFERENCES

- (1) MacDiarmid, A. G.; Chiang, J. C.; Richter, A. F. *Conducting Polymers*; Riedel Publications: Dordrecht, 1987.
- (2) Huang, W. S.; Humphrey, B. D.; MacDiarmid, A. G. *J. Chem. Soc., Faraday Trans. I* **1986**, *82*, 2385–2400.
- (3) MacDiarmid, A. G.; Chiang, J. C.; Richter, A. F.; Epstein, A. J. *Synth. Met.* **1987**, *18*, 285–290.
- (4) Chiang, J. C.; MacDiarmid, A. G. *Synth. Met.* **1986**, *13*, 193–205.
- (5) Epstein, A. J.; Ginder, J. M.; Zuo, F.; Woo, H. S.; Tanner, D. B.; Richter, A. F.; Angelopoulos, M.; Huang, W. S.; MacDiarmid, A. G. *Synth. Met.* **1987**, *21*, 63–70.
- (6) Stafstrom, S.; Bredas, J. L.; Epstein, A. J.; Woo, H. S.; Tanner, D. B.; Huang, W. S.; MacDiarmid, A. G. *Phys. Rev. Lett.* **1987**, *59*, 1464–1467.
- (7) Heeger, A. J. *Synth. Met.* **2001**, *125*, 23–42.
- (8) Huang, J. X.; Virji, S.; Weiller, B. H.; Kaner, R. B. *J. Am. Chem. Soc.* **2003**, *125*, 314–315.
- (9) Hangarter, C. M.; Bangar, M.; Mulchandani, A.; Myung, N. V. *J. Mater. Chem.* **2010**, *20*, 3131–3140.
- (10) Virji, S.; Huang, J. X.; Kaner, R. B.; Weiller, B. H. *Nano Lett.* **2004**, *4*, 491–496.
- (11) Janata, J.; Josowicz, M. *Nat. Mater.* **2003**, *2*, 19–24.
- (12) Li, P.; Tan, T. C.; Lee, J. Y. *Synth. Met.* **1997**, *88*, 237–242.
- (13) Barbero, C.; Miras, M. C.; Schnyder, B.; Haas, O.; Kotz, R. J. *Mater. Chem.* **1994**, *4*, 1775–1783.
- (14) Ponzio, E. A.; Benedetti, T. M.; Torresi, R. M. *Electrochim. Acta* **2007**, *52*, 4419–4427.
- (15) Varela, H.; Huguenin, F.; Malta, M.; Torresi, R. M. *Quim. Nova* **2002**, *25*, 287–299.
- (16) Venkatachalam, S.; Prabhakaran, P. V. *Synth. Met.* **1998**, *97*, 141–146.
- (17) Cromack, K. R.; Jozefowicz, M. E.; Ginder, J. M.; Epstein, A. J.; McCall, R. P.; Du, G.; Leng, J. M.; Kim, K.; Li, C.; Wang, Z. H.; et al. *Macromolecules* **1991**, *24*, 4157–4161.
- (18) Li, Z. F.; Kang, E. T.; Neoh, K. G.; Tan, K. L. *Synth. Met.* **1997**, *87*, 45–52.
- (19) Paul, R. K.; Pillai, C. K. S. *Polym. Int.* **2001**, *50*, 381–386.
- (20) Traore, M. K.; Stevenson, W. T. K.; McCormick, B. J.; Dorey, R. C.; Wen, S.; Meyers, D. *Synth. Met.* **1991**, *40*, 137–153.
- (21) Zeng, X.-R.; Ko, T.-M. *Polymer* **1998**, *39*, 1187–1195.
- (22) Bhadra, S.; Khastgir, D. *Polym. Degrad. Stab.* **2008**, *93*, 1094–1099.
- (23) Chen, C.-H. *J. Polym. Sci., Pt. B: Polym. Phys.* **2003**, *41*, 2142–2148.
- (24) Conklin, J. A.; Huang, S. C.; Huang, S. M.; Wen, T. L.; Kaner, R. B. *Macromolecules* **1995**, *28*, 6522–6527.
- (25) Ding, L.; Wang, X.; Gregory, R. V. *Synth. Met.* **1999**, *104*, 73–78.
- (26) Wei, Y.; Jang, G.-W.; Hsueh, K. F.; Scherr, E. M.; MacDiarmid, A. G.; Epstein, A. J. *Polymer* **1992**, *33*, 314–322.
- (27) Luo, K.; Shi, N.; Sun, C. *Polym. Degrad. Stab.* **2006**, *91*, 2660–2664.
- (28) Mathew, R.; Mattes, B. R.; Espe, M. P. *Synth. Met.* **2002**, *131*, 141–147.
- (29) Tsocheva, D.; Zlatkov, T.; Terlemezyan, L. *J. Therm. Anal. Calorim.* **1998**, *53*, 895–904.
- (30) Do Nascimento, G. M.; Silva, C. H. B.; Temperini, M. L. A. *Polym. Degrad. Stab.* **2008**, *93*, 291–297.
- (31) da Silva, J. E. P.; de Faria, D. L. A.; de Torresi, S. I. C.; Temperini, M. L. A. *Macromolecules* **2000**, *33*, 3077–3083.
- (32) Sedenkova, I.; Trchova, M.; Stejskal, J. *Polym. Degrad. Stab.* **2008**, *93*, 2147–2157.
- (33) Tan, H. H.; Neoh, K. G.; Liu, F. T.; Kocherginsky, N.; Kang, E. T. *J. Appl. Polym. Sci.* **2001**, *80*, 1–9.
- (34) Amano, K.; Ishikawa, H.; Kobayashi, A.; Satoh, M.; Hasegawa, E. *Synth. Met.* **1994**, *62*, 229–232.
- (35) Hagiwara, T.; Yamaura, M.; Iwata, K. *Synth. Met.* **1988**, *25*, 243–252.
- (36) Kulkarni, V. G.; Campbell, L. D.; Mathew, W. R. *Synth. Met.* **1989**, *30*, 321–325.
- (37) Do Nascimento, G. M.; da Silva, J. E. P.; de Torresi, S. I. C.; Temperini, M. L. A. *Macromolecules* **2002**, *35*, 121–125.
- (38) Prokes, J.; Stejskal, J. *Polym. Degrad. Stab.* **2004**, *86*, 187–195.
- (39) Scherr, E. M.; MacDiarmid, A. G.; Manohar, S. K.; Masters, J. G.; Sun, Y.; Tang, X.; Druy, M. A.; Glatkowski, P. J.; Cajipe, V. B.; Fischer, J. E.; et al. *Synth. Met.* **1991**, *41*, 735–738.
- (40) da Silva, J. E. P.; de Torresi, S. I. C.; Temperini, M. L. A. *J. Braz. Chem. Soc.* **2000**, *11*, 91–94.
- (41) MacDiarmid, A. G.; Min, Y.; Wiesinger, J. M.; Oh, E. J.; Scherr, E. M.; Epstein, A. J. *Synth. Met.* **1993**, *55*, 753–760.
- (42) Genies, E. M.; Lapkowski, M.; Penneau, J. F. *J. Electroanal. Chem.* **1988**, *249*, 97–107.
- (43) Mentus, S.; Ciric-Marjanovic, G.; Trchova, M.; Stejskal, J. *Nanotechnology* **2009**, *20*, 245601.
- (44) Wu, L. L.; Luo, J.; Lin, Z. H. *J. Electroanal. Chem.* **1996**, *417*, 53–58.
- (45) Furukawa, Y.; Ueda, F.; Hyodo, Y.; Harada, I.; Nakajima, T.; Kawagoe, T. *Macromolecules* **1988**, *21*, 1297–1305.
- (46) Louarn, G.; Lapkowski, M.; Quillard, S.; Pron, A.; Buisson, J. P.; Lefrant, S. *J. Phys. Chem.* **1996**, *100*, 6998–7006.
- (47) Gruger, A.; Novak, A.; Regis, A.; Colomban, P. *J. Mol. Struct.* **1994**, *328*, 153–167.
- (48) Boyer, M. I.; Quillard, S.; Louarn, G.; Froyer, G.; Lefrant, S. *J. Phys. Chem. B* **2000**, *104*, 8952–8961.
- (49) Cochet, M.; Louarn, G.; Quillard, S.; Buisson, J. P.; Lefrant, S. *J. Raman Spectrosc.* **2000**, *31*, 1041–1049.
- (50) Izumi, C. M. S.; Ferreira, A. M. C.; Constantino, V. R. L.; Temperini, M. L. A. *Macromolecules* **2007**, *40*, 3204–3212.
- (51) Izumi, C. M. S.; Ferreira, D. C.; Ferreira, A. M. C.; Temperini, M. L. A. *Synth. Met.* **2009**, *159*, 1165–1173.
- (52) Ferreira, D. C.; Pires, J. R.; Temperini, M. L. A. *J. Phys. Chem. B* **2011**, *115*, 1368–1375.
- (53) Do Nascimento, G. M.; Silva, C. H. B.; Temperini, M. L. A. *Macromol. Rapid Commun.* **2006**, *27*, 255–259.
- (54) Do Nascimento, G. M.; Silva, C. H. B.; Izumi, C. M. S.; Temperini, M. L. A. *Spectrochim. Acta, Part A* **2008**, *71*, 869–875.
- (55) Do Nascimento, G. M.; Constantino, V. R. L.; Landers, R.; Temperini, M. L. A. *Macromolecules* **2004**, *37*, 9373–9385.
- (56) Izumi, C. M. S.; Constantino, V. R. L.; Temperini, M. L. A. *J. Phys. Chem. B* **2005**, *109*, 22131–22140.
- (57) Izumi, C. M. S.; Constantino, V. R. L.; Temperini, M. L. A. *J. Nanosci. Nanotechnol.* **2007**, *8*, 1782–1789.
- (58) Fou, A. C.; Rubner, M. F. *Macromolecules* **1995**, *28*, 7115–7120.

- (59) Cheung, J. H.; Stockton, W. B.; Rubner, M. F. *Macromolecules* **1997**, *30*, 2712–2716.
- (60) Moon, D. K.; Ezuka, M.; Maruyama, T.; Osakada, K.; Yamamoto, T. *Macromolecules* **1993**, *26*, 364–369.
- (61) Le Ru, E. C.; Blackie, E.; Meyer, M.; Etchegoin, P. G. *J. Phys. Chem. C* **2007**, *111*, 13794–13803.
- (62) Frisch, M. J.; Trucks, G. W.; Schlegel, H. B.; Scuseria, G. E.; Robb, M. A.; Cheeseman, J. R.; Montgomery, J. A.; Vreven, T. J.; Kudin, K. N.; Burant, J. C.; et al. *Gaussian 03*, rev D.01; Gaussian, Inc.: Wallingford, CT, 2004.
- (63) Becke, A. D. *J. Chem. Phys.* **1993**, *98*, 5648–5652.
- (64) Lee, C. T.; Yang, W. T.; Parr, R. G. *Phys. Rev. B* **1988**, *37*, 785–789.
- (65) Stephens, P. J.; Devlin, F. J.; Chabalowski, C. F.; Frisch, M. J. *J. Phys. Chem.* **1994**, *98*, 11623–11627.
- (66) Merrick, J. P.; Moran, D.; Radom, L. *J. Phys. Chem. A* **2007**, *111*, 11683–11700.
- (67) Zvereva, E. E.; Shagidullin, A. R.; Katsyuba, S. A. *J. Phys. Chem. A* **2011**, *115*, 63–69.
- (68) Ciric-Marjanovic, G.; Blinova, N. V.; Trchova, M.; Stejskal, J. *J. Phys. Chem. B* **2007**, *111*, 2188–2199.
- (69) Ciric-Marjanovic, G.; Trchova, M.; Konyushenko, E. N.; Holler, P.; Stejskal, J. *J. Phys. Chem. B* **2008**, *112*, 6976–6987.
- (70) Ciric-Marjanovic, G.; Trchova, M.; Stejskal, J. *J. Raman Spectrosc.* **2008**, *39*, 1375–1387.
- (71) Folch, S.; Regis, A.; Gruger, A.; Colombari, P. *Synth. Met.* **2000**, *110*, 219–227.
- (72) Furukawa, Y.; Hara, T.; Hyodo, Y.; Harada, I. *Synth. Met.* **1986**, *16*, 189–198.
- (73) da Silva, J. E. P.; Temperini, M. L. A.; de Torresi, S. I. C. *Electrochim. Acta* **1999**, *44*, 1887–1891.
- (74) Lee, K.; Heeger, A. J.; Cao, Y. *Synth. Met.* **1995**, *72*, 25–34.
- (75) MacDiarmid, A. G.; Epstein, A. J. *Synth. Met.* **1994**, *65*, 103–116.
- (76) Huang, W. S.; MacDiarmid, A. G. *Polymer* **1993**, *34*, 1833–1845.
- (77) Stafstrom, S.; Sjogren, B.; Bredas, J. L. *Synth. Met.* **1989**, *29*, E219–E226.
- (78) Izumi, C. M. S.; Andrade, G. F. S.; Temperini, M. L. A. *J. Phys. Chem. B* **2008**, *112*, 16334–16340.
- (79) Silva, C. H. B.; Ferreira, D. C.; Constantino, V. R. L.; Temperini, M. L. A. *J. Raman Spectrosc.* **2011**, *42*, 1653–1659.
- (80) Durnick, T. J.; Wait, S. C. *J. Mol. Spectrosc.* **1972**, *42*, 211–226.
- (81) Takahashi, M.; Goto, M.; Ito, M. *Chem. Phys. Lett.* **1985**, *121*, 458–463.